Mechanics of Materials 165 (2022) 104134

Contents lists available at ScienceDirect

Mechanics of Materials

journal homepage: www.elsevier.com/locate/mecmat

Research paper

Machine learning based inverse modeling of full-field strain distribution for mechanical characterization of a linear elastic and heterogeneous membrane

Yuan Zhang [a], Lin Guo [a], Clement J.A. Brousse [a], Chung-Hao Lee [b], Aurelie Azoug [a], Hongbing Lu [c], Shuodao Wang [a,*]

[a] School of Mechanical and Aerospace Engineering, Oklahoma State University, Stillwater, OK 74074, USA
[b] School of Aerospace and Mechanical Engineering, The University of Oklahoma, Norman, OK 73019, USA
[c] Department of Mechanical Engineering, The University of Texas at Dallas, Richardson, TX 75080, USA

ARTICLE INFO

Keywords:
Heterogeneous membrane
Inverse method
FEA
Machine learning

ABSTRACT

Heterogeneous membranes or films are thin and soft structures with spatial variations in material property and thickness. Mechanical behavior of heterogeneous membranes is not well understood, mainly due to the difficulty in obtaining accurate and reliable material property data. To understand the mechanical behavior of these materials, accurate and efficient characterization methods for heterogeneous membranes are needed. In this paper, an inverse method based on machine learning is developed to efficiently extract mechanical properties from full-field strain distributions. This approach is demonstrated on a flat heterogeneous membrane with uniform thickness formed by up to four linear elastic synthetic materials in a grid arrangement, and deforming in a moderate strain range (true strain ~ 10%). The results show that the machine learning method achieves accuracy comparable to the traditional inverse finite element method, and is 6 orders of magnitude faster in the demonstrated case studies.

1. Introduction

Synthetic thin structures, ranging from non-woven fabrics (Feng, 2017; Nukala, 2016) and thin forms of stretchable/flexible electronics (Rogers et al., 2010; Kim et al., 2011), to foam metals (Fiedler et al., 2006), porous media, and metal alloy systems (Körner and Singer, 2000), are becoming increasingly complex in material composition and thickness variation to meet the demands of multi-functionality, compact designs, and large-scale manufacturing (Chiluka, 2018). Knowing the mechanical properties of these heterogeneous thin products is critical for the optimization of industrial production processes. For example, characterization of the web materials in web-handling will allow predictions of critical buckling loads and help determine important process parameters (Chiluka, 2018).

In addition to synthetic materials, many thin, soft biological tissues (e.g. meninges Gu et al., 2012, eardrums Wang et al., 2017, heart valves Jett et al., 2018, skins Rensink, 2012) are made of different materials, and their thickness varies spatially (Barr, 2014; Asally et al., 2012; Fung, 2013). Due to their small thickness, these synthetic and biological membranes lose structural stability under small compressive or tensile loads.

The mechanical behavior of these heterogeneous materials is not well understood, mainly due to the lack of an efficient characterization method. Some prior studies used a single effective material to represent the entire heterogeneous structure, and extract the effective properties of the heterogeneous material from experimental measurement of force–deformation relations (Forte et al., 2017; Babarenda Gamage et al., 2011). These simplified models ignore the local property variations in heterogeneous structures, which could lead to errors when predicting local structure deformation or failure. Another category of characterization methods, referred to as inverse methods (Cooreman et al., 2008), extracts material properties of heterogeneous structures from the displacement field under given loading conditions. The input of the inverse method is the displacement field which can be obtained by Digital Image Correlation (DIC) (Pan et al., 2009). There are several methods to solve this type of inverse problems (Avril et al., 2008; Martins et al., 2018). For example, the constitutive equation gap method (CEGM) was first developed by Ladevèze and Leguillon in 1983 (Ladeveze and Leguillon, 1983) to estimate the error in Finite Element Analysis (FEA). In 2002, Geymonat, Hild and Pagano adopted this method to identify material parameters from full-field measurements (Geymonat et al., 2002). More recently, CEGM has been applied to study heterogeneous materials (Florentin and Lubineau, 2011), anisotropic elasticity (Guchhait and Banerjee, 2016), and plasticity (Latourte et al., 2008). The advantage of CEGM is its applicability

* Corresponding author.
E-mail address: shuodao.wang@okstate.edu (S. Wang).

https://doi.org/10.1016/j.mechmat.2021.104134
Received 30 June 2021; Received in revised form 4 October 2021; Accepted 1 November 2021
Available online 17 November 2021

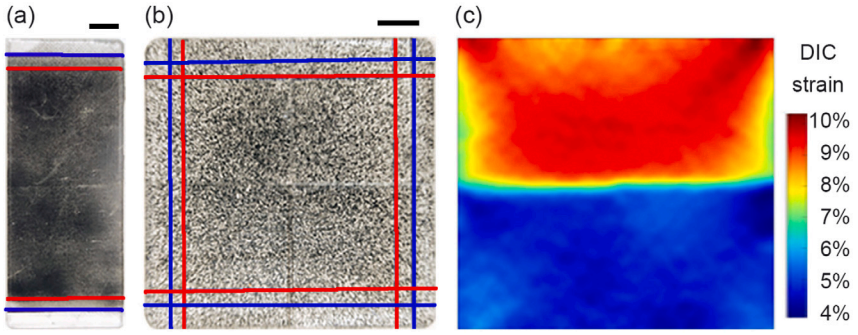

Fig. 1. Fabricated (a) 1 × 2 and (b) 2 × 2 heterogeneous specimens with clamping boundaries (blue lines) and boundaries for area of interests in DIC (red lines). The size bars in the figures represent 10 mm. (c) the full-field strain distribution of a 2 × 2 specimen obtained by 2D DIC. (For interpretation of the references to color in this figure legend, the reader is referred to the web version of this article.)

to any constitutive model. However, the calculation of a statically admissible stress field can be computationally costly, especially when the material is more complex. Another method is the Virtual Fields Method (VFM), first introduced by Grédiac in 1989 (Grédiac, 1989). VFM has superior computational efficiency for homogeneous materials because the virtual strain field can be obtained analytically (Pierron and Grédiac, 2012; Grédiac et al., 2006). However, when the material is heterogeneous, FEA iterations are needed to calculate the virtual strain field using return-mapping algorithms. Another commonly used inverse method is the Finite Element Model Updating (FEMU) method (Kavanagh and Clough, 1971). Kauer et al. (2002) used FEMU to characterize the viscoelastic material properties of a soft tissue. None of the above methods can handle materials with complex heterogeneity or thickness variations, mainly because of high computational costs and difficulties in convergence.

With the fast development of the machine learning (ML) technology (Jordan and Mitchell, 2015; LeCun et al., 2015) in recent years, more and more complex problems (including physics-based problems) can be solved. For example, Hoerig et al. developed an information-based machine learning approach for elasticity imaging of soft biological tissue (Hoerig et al., 2017); Ghaboussi et al. proposed an approach combining the Gappy Proper Orthogonal Decomposition machine learning technique with a physics-based direct inversion strategy for material characterization (Ghaboussi et al., 1998). ML can also be used to study the mechanical behavior of materials (He et al., 2021; Zhang et al., 2019; Bishnoi et al., 2019; Wang and Sun, 2018; Liu et al., 2019; Heider et al., 2020; Ghaboussi et al., 1998, 1991). By applying ML, the efficiency of the inverse solving process is significantly improved. However, there is still a gap of knowledge in applying ML to determine the relationship between heterogeneous material properties and displacement fields.

To advance understanding of the mechanical behavior of thin and heterogeneous materials, this study develops a ML neural network which is trained with FEA generated data. The developed neural network can efficiently extract material properties from full-field experimental strain measurements. The focus of the study is on a thin, flat, and linear elastic heterogeneous membrane with up to four materials in a grid arrangement and deforming in the moderate strain range (true strain ~10%). A comprehensive numerical and experimental study is performed to validate the proposed method.

2. Methodology

In this study, a collection of heterogeneous membranes (polydimethylsiloxane, or PDMS) were fabricated to reach controlled geometry (especially controlled thickness) and material properties. Membranes of 1 × 2 and 2 × 2 grid material patterns were fabricated. Details of the fabrication process are documented in Section 5. The mixing ratio of Sylgard 184 PDMS was varied to create PDMS with Young's moduli between 1.0–3.0 MPa. A Poisson's ratio of 0.49 was assumed for all PDMS materials, so the Young's moduli are the only unknowns in the inverse method.

Two-dimensional (2D) digital image correlation (DIC) technique was then used to measure the full-field displacements of the specimens under uniaxial tensile loading (Peters and Ranson, 1982; Lu and Cary, 2000). The software Ncorr (Blaber et al., 2015) was used to calculate the Green strain distribution from the full-field displacements. The Green strain was converted to logarithmic strain and compared to the strain obtained from the FEA software SIMULIA ABAQUS (SIMULIA ABAQUS). Material properties and thickness of each material in the specimen were experimentally measured right after the tensile testing, and used as inputs for inverse modeling.

Two inverse modeling methods were adopted to extract the material properties from the measured full-field strain distributions — the traditional FEMU and ML-based inverse methods. The two methods are compared for computational efficiency and accuracy in Section 3.

2.1. Full-field strain measurement

After the specimens were fabricated, an airbrush was used to spray a random ink pattern on the surface of the specimens. The 1 × 2 specimens (Fig. 1a) were clamped at the blue lines, and uniaxial tensile tests were performed on an Instron 5942 system. The 2 × 2 specimens (Fig. 1b) were clamped at the top and bottom blue lines and stretched vertically, then released and clamped at the left and right blue lines and stretched horizontally. Each material takes up a 40 × 40 mm^2 area for the 1 × 2 specimens within the area of interest, and a 25 × 25 mm^2 area for the 2 × 2 specimens, so the size and zone of each material are known.

During the tensile tests, videos were recorded by a Nicon D5 camera (Tamron AF 90 mm f/2.8 Di SP AF/MF 1:1 Macro Lens) with a resolution of 3840 × 2160 pixels, and converted into images in MATLAB, with each frame corresponding to a load recorded by the Instron system. DIC was performed to obtain displacements inside the area marked by the red lines, and the full-field strains were calculated by the software Ncorr. For 2 × 2 specimens, after the first tensile test with loading in the vertical direction, the specimens were released, and the tensile testing was repeated with loading in the horizontal direction. Two strain fields corresponding to the two stretching directions were determined. The strains corresponding to the same force (10 Newton for 1 × 2 and 16 Newton for 2 × 2 specimens) were used in both the DIC experiments and the inverse modeling.

2.2. Traditional FEMU method

2D FEA models with the same geometry and material domains as in the physical specimens were developed for the FEMU method.

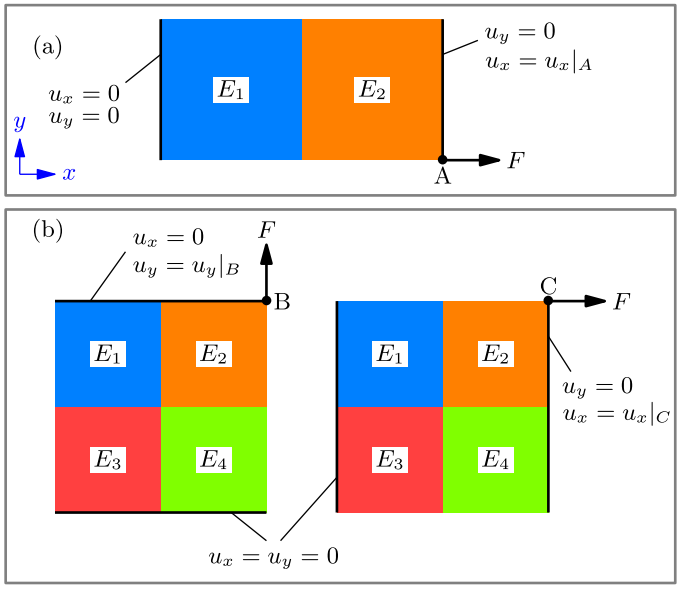

Fig. 2. 2D FEA models for (a) 1 × 2 and (b) 2 × 2 specimens. The stretching forces are applied on the control nodes A, B, and C. For the boundary nodes, the displacements in the stretching direction are coupled to the control nodes to simulate a clamped condition.

The boundary conditions corresponding to the clamped–clamped constraints in experiments are depicted in Fig. 2. For the 1 × 2 specimens, a single model was needed, while for the 2 × 2 specimens, two models were simulated simultaneously to fit the two strain fields of the same specimen being stretched in x and y directions, respectively. The materials were treated as linear elastic with a fixed Poison's ratio of 0.49. The sizes and zone of each material were fixed and consistent with the physical specimens. Geometric nonlinearity was considered in the forward solving FEA process.

A rigorous algorithm was implemented in the extended CAE suite by SIMULIA. Specifically, the Isight and the SIMULIA Execution Engine was used for creating simulation process flows consisting of a series of integrated and automatic FEA simulation, data matching, and optimization processes. This process flow iteratively changes the material parameters to fit an experimentally obtained full-field strain distribution. The optimization was performed in Isight to search for the optimal material parameter set that minimizes the mean squared error (MSE) between the simulated strain distribution and the DIC experiment. For the FEMU method, several optimization methods, including Downhill Simplex, Hooke–Jeeves, and Multi-Island GA, were tested for the same task. The Downhill Simplex method was selected for having the best efficiency among the three. Several different combinations of initial guess were also tested, the results show there is no significant influence on the convergence time or the converged values. Isight was set to run 100 iterations then the MSE was calculated to evaluate the quality of the solution. A MSE between predicted and experimental strains of $< 2 \times 10^{-4}$ was considered acceptable in this study.

2.3. Inverse modeling using machine learning

Contrast to the traditional method that manipulates the material parameters in the governing equations to derive a solution for the inverse elasticity problem (Cooreman et al., 2008), the ML method learns the pattern from the given training samples and makes predictions for testing samples of the same kind (Hagan et al., 2014; LeCun et al., 1998). To solve the inverse moduli mapping problem, an FEA generated solution data set was used as the training data to train a neural network to approximate the relation between the system response (in this case, full-field strain distribution under a given load) and the inverse unknowns (the Young's moduli). Once the network was developed and trained, the solving process became highly efficient.

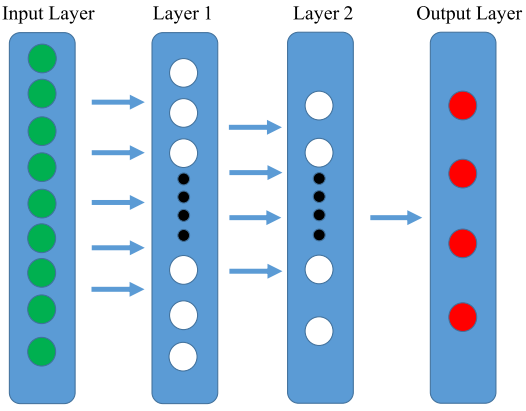

Fig. 3. The architecture of the developed FCNN neural network (Ghaboussi et al., 1991). The input is the full-field strain distribution under a given load, the target is the determination of Young's moduli of all materials. 600 neurons were used in Layer 1 and 200 neurons in Layer 2.

The deep neural network architecture adopted in this study is shown in Fig. 3. A light-weighted Fully Connected Neural Network (FCNN) (Ghaboussi et al., 1991) was designed for the task. The network parameters were set heuristically so that the network is capable of handling the inverse problem with a low computational cost. The strain of each element in a specimen was used as the input and mapped to a vector before feeding into the network. The moduli of all the materials were estimated in the output layer. The network consists of two linear hidden layers before the output. 600 neurons were used in Layer 1 and 200 neurons in Layer 2. The network was trained for 60,000 epochs with the loss function defined as the MSE between the output (predicted moduli) and the ground-truth moduli (given by the training data set). The neuron learning rate decayed with a factor of 0.9 for each 10,000 epochs in the training process to allow adjustments to improve the network-data fitting. The neuron parameters were updated automatically during training to minimize the MSE loss to ensure that the network produces accurate moduli predictions. The ML results showed that the trained network was capable of handling both 1 × 2 and 2 × 2 moduli predictions.

Table 1
Comparison of Young's modulus values for 1 × 2 specimens.

		Experiment	Thickness	FEMU		ML	
		(MPa)	(mm)	(MPa)	Error (%)	(MPa)	Error (%)
Specimen 1	E_1	1.83 ± 0.031	1.76 ± 0.025	1.90	4.27	1.79	1.94
	E_2	2.59 ± 0.048	1.82 ± 0.038	2.72	4.87	2.60	0.22
Specimen 2	E_1	1.30 ± 0.016	1.87 ± 0.018	1.36	4.68	1.24	4.64
	E_2	2.56 ± 0.081	1.95 ± 0.018	2.69	5.06	2.54	0.72
Specimen 3	E_1	2.93 ± 0.054	1.95 ± 0.015	3.03	3.20	2.97	1.34
	E_2	1.55 ± 0.029	1.83 ± 0.018	1.63	5.05	1.55	0.323
Specimen 4	E_1	2.92 ± 0.050	1.87 ± 0.022	3.05	4.44	2.97	1.68
	E_2	1.32 ± 0.059	1.76 ± 0.036	1.37	3.84	1.23	6.84
Specimen 5	E_1	2.72 ± 0.044	2.10 ± 0.061	2.69	0.785	2.67	1.67
	E_2	1.26 ± 0.024	2.18 ± 0.047	1.20	4.91	1.23	2.56

Table 2
Comparison of Young's modulus values for 2 × 2 specimens.

		Experiment	Thickness	FEMU		ML	
		(MPa)	(mm)	(MPa)	Error (%)	(MPa)	Error (%)
Specimen 1	E_1	2.14 ± 0.099	1.90 ± 0.061	2.23	4.30	2.19	2.25
	E_2	1.81 ± 0.033	1.98 ± 0.016	1.83	1.24	1.81	0.12
	E_3	0.99 ± 0.014	1.97 ± 0.009	1.01	1.81	1.04	4.78
	E_4	1.32 ± 0.030	1.97 ± 0.043	1.35	1.92	1.34	1.37
Specimen 2	E_1	1.55 ± 0.008	1.90 ± 0.065	1.60	3.70	1.53	1.04
	E_2	1.11 ± 0.011	1.96 ± 0.004	1.10	0.12	1.08	2.22
	E_3	2.67 ± 0.030	1.92 ± 0.030	2.78	4.33	2.67	0.318
	E_4	1.97 ± 0.021	1.85 ± 0.043	2.04	3.88	1.97	0.267
Specimen 3	E_1	1.94 ± 0.070	2.22 ± 0.025	1.92	1.28	1.93	0.467
	E_2	1.25 ± 0.032	2.01 ± 0.065	1.28	2.51	1.22	2.72
	E_3	2.93 ± 0.084	2.08 ± 0.053	3.03	3.38	2.90	1.28
	E_4	1.37 ± 0.061	2.07 ± 0.048	1.36	1.19	1.34	2.49
Specimen 4	E_1	2.75 ± 0.078	2.01 ± 0.008	2.88	4.81	2.73	0.909
	E_2	1.52 ± 0.074	1.94 ± 0.059	1.60	4.76	1.50	1.43
	E_3	1.99 ± 0.029	2.10 ± 0.046	1.99	0.0010	1.95	2.04
	E_4	1.17 ± 0.038	2.12 ± 0.021	1.12	4.19	1.15	1.30
Specimen 5	E_1	1.04 ± 0.039	2.03 ± 0.015	1.01	2.93	1.04	0.446
	E_2	2.22 ± 0.044	2.04 ± 0.007	2.32	4.57	2.20	0.953
	E_3	1.42 ± 0.039	1.86 ± 0.019	1.49	4.52	1.40	1.75
	E_4	3.14 ± 0.015	1.84 ± 0.025	3.25	3.21	3.17	0.708

To generate the network training data, an FEA model with about 7000 elements was established with the same material pattern as the experimental specimens. Assuming the materials' moduli are within the range of 0.75–3.5 MPa, a large number of Young's moduli combinations which cover the whole search space were generated as the training data set. This enables the network to handle any possible combination. Specifically, the moduli combinations (E_1, E_2 in Fig. 2a can take any value in the set [0.75, 0.85, …, 3.45, 3.5] MPa, i.e. a total of 841 possible combinations for 1 × 2 specimens; E_1, E_2, E_3, and E_4 in Fig. 2b can take any value in the set [0.75, 1.25, 1.75, …, 3.25] MPa, i.e. a total of 1296 possible combinations for 2 × 2 specimens) were assigned to each specimen, and the corresponding logarithmic strain distribution of all the elements was computed by FEA. Under a set force (10 Newton for 1 × 2 and 16 Newton for 2 × 2 specimens), the strains were used as the training inputs and the Young's moduli were used as training output targets. 500 synthetic validation data with random Young's moduli were also prepared to evaluate the network performance. The network was built and tested using NVIDIA GTX 750 ti graphic card with 640 CUDA cores. The training time varied according to the network parameters, the number of element in the FEA model, and the number of specimens in the training set. For example, the 1 × 2 case with 841 samples in the training set needed a training time of approximately 15 min. The testing accuracy on randomly synthetic samples reached <0.4% error on average. Once the network was developed and fully trained, it only took 1 ms to generate the required output for any new input (full-field strain distributions) obtained from FEA generated data or DIC experiments.

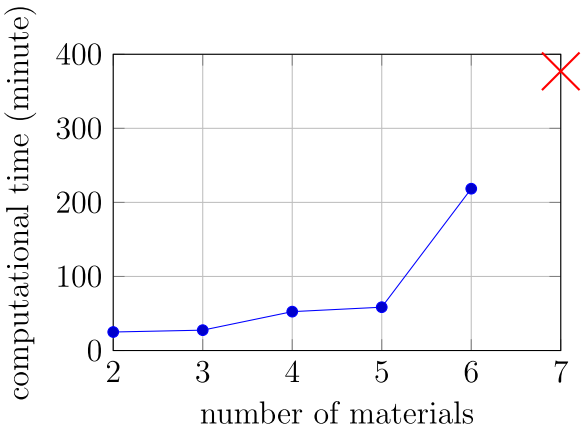

Fig. 4. The computational time needed to reach convergence (MSE≤0.0025) versus the number of unknown materials for the $1 \times N$ cases. The $N = 7$ case is not converged (red cross) after more than 6 h of computational time.

3. Results and discussions

3.1. Accuracy of the FEMU and ML methods

The results of the two inverse modeling methods – FEMU by Abaqus Isight and ML – are given in Tables 1 and 2. Both methods can extract the material properties accurately, with errors up to ~5% from the experimentally measured average modulus. It is noted that the average experimental values are also subject to measurement errors (the standard deviations of four measurements are given in the tables). The MSE between predicted and experimental strains for the FEMU method in all the cases is $< 2 \times 10^{-4}$ after 100 iterations.

3.2. Efficiency comparison between the FEMU and ML methods

For the 2 × 2 specimens, the time FEMU needed for each inverse problem was about 30 min (with an AMD FX-8350 8-core CPU). In comparison, the time used to train the neural network was only about 15 minutes (with NVIDIA GTX 750 ti with 640 CUDA cores GPU). After the training is completed, the network took merely ~1 ms (this will not be significantly affected by hardware) to solve an inverse problem from any given strain field. The training process is only needed once, then the trained ML network performs a one-step feed-forward calculation to efficiently predict the moduli for any new specimen. On the other hand, the FEMU is an optimization-based iterative approach that has limited performance. The inverse solving process of the ML method was 6 orders of magnitude faster than FEMU in the current study. It should be noted that with careful additional adjustments to the FEMU inverse method such as adjoint formulation or Gauss–Newton procedures, the efficiency of the FEMU method may be increased, but it will still have potential problems of slow convergence or converging to local minima (Gokhale et al., 2008; Goenezen et al., 2011; Guchhait and Banerjee, 2015; Oberai et al., 2009).

3.3. Limitation of the FEMU method

Noting that the FEMU method was difficult to converge for the 2 × 2 cases, a set of numerical experiments were designed to test the efficiency of the solving method. Here a $1 \times N$ material pattern was designed, and the strain field corresponding to a set of materials was calculated by FEA and used as "virtual experimental" data. The FEMU was then used to inversely calculate the moduli from the given strain field. It is found that for simulations with less than 6 unknown material parameters, the FEMU produced accurate predictions with a maximum

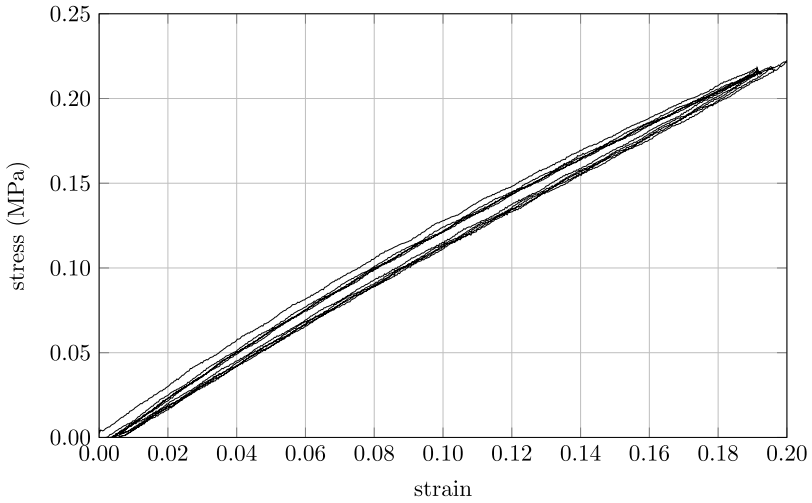

Fig. 5. Approximate linear, elastic response of PDMS under 5 loading/unloading cycles with maximum strain of 20% and strain rate of 0.5%/min.

error of 0.054%. However, for the 1×6 case, the maximum error was 1.6%. The computational time also increased significantly when the number of materials in a specimen was greater than 5, and convergence became extremely difficult when the number of materials was greater than 6 (Fig. 4, the red cross represents a non-converged case). It is clear that the efficiency and accuracy of the FEMU method decreases significantly with the increase of the number of materials. Therefore, in future studies when the geometry becomes more complex, and/or the number of unknown parameters increases, FEMU might not be able to solve those problems, but the ML-based inverse method can still provide a solution.

4. Conclusions and future studies

A ML-based inverse method is developed to determine the material parameters in a linear elastic and heterogeneous membrane. The method is demonstrated on flat specimens. The conclusions of this study are summarized below:

1. Both the FEMU and ML inverse methods are capable of inversely solving moduli of heterogeneous membranes from full-field strain distributions obtained from 2D DIC, with accuracy within $\sim 5\%$ of the experimentally measured moduli.
2. ML is as accurate as the traditional FEMU method, but has a significant advantage in terms of computational efficiency. The training time is negligible, and the required number of data sets is moderate for these case studies. The computational time is 6 orders of magnitude less than that of FEMU for the 2×2 heterogeneous patterns.
3. The network structure will be further optimized in future studies to increase the efficiency of the training process and reduce the prediction error. Deep learning techniques will be implemented to make the network more robust for noisy DIC data.
4. Future studies will focus on enabling the ML neural network to learn the relationships between given loads and moduli, as well as extending its capability from handling simple patterns to more complex patterns (e.g. from 2×2 to 4×4, and eventually being able to handle any desired resolution of $M \times N$). When the number of unknown materials ML can handle increases to sufficiently large, this method can be used to characterize complex heterogeneous membranes.

5. Experiments

5.1. Specimen fabrication

PDMS Sylgard 184 was processed to make specimens of different Young's moduli. Molds of specified geometries were created with 3D printers and a milling machine. The PDMS base and curing agent were mixed at a chosen weight ratio by a mixing machine for 15 min. The mixture was degassed in a vacuum chamber for 60 min. The mold surface was sprayed with a mold release agent, and the mixture was cast into the mold. Specimens were then cured in an oven (100 °C) for 5 h. Once fully cured, specimens were cooled down to room temperature. For heterogeneous specimens, each material was cast and cured sequentially – e.g. for the 1×2 specimens, the first material was cast to fill the whole mold and cured, then the specimen was cut into 2 halves and one of them was used to fill half of the mold. Lastly, the second material was cast and cured. This method created heterogeneous specimens with strong material interfaces such that the material interfaces did not fracture during the tensile testing.

5.2. Linearity of PDMS under true strain <20%

PDMS Sylgard 184 under various compound mixing ratios were made into single-material testing coupons. The strain and stress data under a uniaxial tensile test (strain rate 5%/min) was plotted, and the slopes were fitted with MATLAB to obtain the Young's moduli. Tensile tests with repeated loading and unloading cycles were performed to check the elastic linearity. Results showed that PDMS Sylgard 184 can be treated as a linear elastic material for strains up to 20% as shown in Fig. 5.

5.3. Experimental measurement of single-material moduli

It was also found that the PDMS's Young's modulus is highly dependent on the mixing ratio, the curing temperature, and the resting time before tensile test. The modulus of each constituent in the heterogeneous specimens were measured right after the uniaxial testing. The heterogeneous specimens were cut into coupons of single-material, and for each material, 4 coupons were prepared and tested, and the obtained moduli were averaged.

Declaration of competing interest

The authors declare that they have no known competing financial interests or personal relationships that could have appeared to influence the work reported in this paper.

Acknowledgments

S. Wang acknowledges the support of the NSF CAREER, United States Award CMMI-1847062 and the Oklahoma Center for Advancement of Science & Technology Grant HR18-085; H. Lu acknowledges the support of NSF, United States under CMMI-1661246 & CMMI-1726435, DOE, United States DE-NA 0003962, and the Louis A. Beachel Jr. Chair.

All authors approved the version of the manuscript to be published.

References

Asally, M., Kittisopikul, M., Rué, P., Du, Y., Hu, Z., Çağatay, T., Robinson, A.B., Lu, H., Garcia-Ojalvo, J., Süel, G.M., 2012. Localized cell death focuses mechanical forces during 3D patterning in a biofilm. Proc. Natl. Acad. Sci. 109 (46), 18891–18896.

Avril, S., Bonnet, M., Bretelle, A.-S., Grédiac, M., Hild, F., Ienny, P., Latourte, F., Lemosse, D., Pagano, S., Pagnacco, E., et al., 2008. Overview of identification methods of mechanical parameters based on full-field measurements. Exp. Mech. 48 (4), 381–402.

Babarenda Gamage, T.P., Rajagopal, V., Ehrgott, M., Nash, M.P., Nielsen, P.M., 2011. Identification of mechanical properties of heterogeneous soft bodies using gravity loading. Int. J. Numer. Methods Biomed. Eng. 27 (3), 391–407.

Barr, R.G., 2014. Elastography in clinical practice. Radiol. Clin. 52 (6), 1145–1162.

Bishnoi, S., Singh, S., Ravinder, R., Bauchy, M., Gosvami, N.N., Kodamana, H., Krishnan, N.A., 2019. Predicting Young's modulus of oxide glasses with sparse datasets using machine learning. J. Non-Cryst. Solids 524, 119643.

Blaber, J., Adair, B., Antoniou, A., 2015. Ncorr: open-source 2D digital image correlation matlab software. Exp. Mech. 55 (6), 1105–1122.

Chiluka, P., 2018. Effects of Non-Uniformity on Trough Instability in Nonwovens (Ph.D. thesis).

Cooreman, S., Lecompte, D., Sol, H., Vantomme, J., Debruyne, D., 2008. Identification of mechanical material behavior through inverse modeling and DIC. Exp. Mech. 48 (4), 421–433.

Feng, J., 2017. Preparation and properties of poly (lactic acid) fiber melt blown non-woven disordered mats. Mater. Lett. 189, 180–183.

Fiedler, T., Pesetskaya, E., Öchsner, A., Grácio, J., 2006. Calculations of the thermal conductivity of porous materials. In: Materials Science Forum, Vol. 514. Trans Tech Publ, pp. 754–758.

Florentin, E., Lubineau, G., 2011. Using constitutive equation gap method for identification of elastic material parameters: technical insights and illustrations. Int. J. Interact. Des. Manuf. (IJIDeM) 5 (4), 227–234.

Forte, A.E., Gentleman, S.M., Dini, D., 2017. On the characterization of the heterogeneous mechanical response of human brain tissue. Biomech. Model. Mechanobiol. 16 (3), 907–920.

Fung, Y., 2013. Biomechanics: Mechanical Properties of Living Tissues. Springer New York.

Geymonat, G., Hild, F., Pagano, S., 2002. Identification of elastic parameters by displacement field measurement. C. R. Méc. 330 (6), 403–408.

Ghaboussi, J., Garrett, Jr., J., Wu, X., 1991. Knowledge-based modeling of material behavior with neural networks. J. Eng. Mech. 117 (1), 132–153.

Ghaboussi, J., Pecknold, D.A., Zhang, M., Haj-Ali, R.M., 1998. Autoprogressive training of neural network constitutive models. Internat. J. Numer. Methods Engrg. 42 (1), 105–126.

Goenezen, S., Barbone, P., Oberai, A.A., 2011. Solution of the nonlinear elasticity imaging inverse problem: The incompressible case. Comput. Methods Appl. Mech. Engrg. 200 (13–16), 1406–1420.

Gokhale, N.H., Barbone, P.E., Oberai, A.A., 2008. Solution of the nonlinear elasticity imaging inverse problem: the compressible case. Inverse Problems 24 (4), 045010.

Grédiac, M., 1989. Principe des travaux virtuels et identification. C. R. Acad. Sci. 309, 1–5, (in French with Abridged English Version).

Grédiac, M., Pierron, F., Avril, S., Toussaint, E., 2006. The virtual fields method for extracting constitutive parameters from full-field measurements: a review. Strain 42 (4), 233–253.

Gu, L., Chafi, M.S., Ganpule, S., Chandra, N., 2012. The influence of heterogeneous meninges on the brain mechanics under primary blast loading. Composites B 43 (8), 3160–3166.

Guchhait, S., Banerjee, B., 2015. Constitutive error based material parameter estimation procedure for hyperelastic material. Comput. Methods Appl. Mech. Engrg. 297, 455–475.

Guchhait, S., Banerjee, B., 2016. Anisotropic linear elastic parameter estimation using error in the constitutive equation functional. Proc. R. Soc. A 472 (2192), 20160213.

Hagan, M.T., Demuth, H.B., Beale, M.H., De Jesus, O., 2014. Neural Network Design, second ed. Martin Hagan Publication.

He, Q., Laurence, D.W., Lee, C.-H., Chen, J.-S., 2021. Manifold learning based data-driven modeling for soft biological tissues. J. Biomech. 117, 110124.

Heider, Y., Wang, K., Sun, W., 2020. SO (3)-invariance of informed-graph-based deep neural network for anisotropic elastoplastic materials. Comput. Methods Appl. Mech. Engrg. 363, 112875.

Hoerig, C., Ghaboussi, J., Insana, M.F., 2017. An information-based machine learning approach to elasticity imaging. Biomech. Model. Mechanobiol. 16 (3), 805–822.

Jett, S., Laurence, D., Kunkel, R., Babu, A.R., Kramer, K., Baumwart, R., Towner, R., Wu, Y., Lee, C.-H., 2018. An investigation of the anisotropic mechanical properties and anatomical structure of porcine atrioventricular heart valves. J. Mech. Behav. Biomed. Mater. 87, 155–171.

Jordan, M.I., Mitchell, T.M., 2015. Machine learning: Trends, perspectives, and prospects. Science 349 (6245), 255–260.

Kauer, M., Vuskovic, V., Dual, J., Székely, G., Bajka, M., 2002. Inverse finite element characterization of soft tissues. Med. Image Anal. 6 (3), 275–287.

Kavanagh, K.T., Clough, R.W., 1971. Finite element applications in the characterization of elastic solids. Int. J. Solids Struct. 7 (1), 11–23.

Kim, D.-H., Lu, N., Ma, R., Kim, Y.-S., Kim, R.-H., Wang, S., Wu, J., Won, S.M., Tao, H., Islam, A., et al., 2011. Epidermal electronics. Science 333 (6044), 838–843.

Körner, C., Singer, R.F., 2000. Processing of metal foams—challenges and opportunities. Adv. Energy Mater. 2 (4), 159–165.

Ladeveze, P., Leguillon, D., 1983. Error estimate procedure in the finite element method and applications. SIAM J. Numer. Anal. 20 (3), 485–509.

Latourte, F., Chrysochoos, A., Pagano, S., Wattrisse, B., 2008. Elastoplastic behavior identification for heterogeneous loadings and materials. Exp. Mech. 48 (4), 435–449.

LeCun, Y., Bengio, Y., Hinton, G., 2015. Deep learning. Nature 521 (7553), 436–444.

LeCun, Y., Bottou, L., Bengio, Y., Haffner, P., 1998. Gradient-based learning applied to document recognition. Proc. IEEE 86 (11), 2278–2324.

Liu, Z., Wu, C., Koishi, M., 2019. A deep material network for multiscale topology learning and accelerated nonlinear modeling of heterogeneous materials. Comput. Methods Appl. Mech. Engrg. 345, 1138–1168.

Lu, H., Cary, P., 2000. Deformation measurements by digital image correlation: implementation of a second-order displacement gradient. Exp. Mech. 40 (4), 393–400.

Martins, J., Andrade-Campos, A., Thuillier, S., 2018. Comparison of inverse identification strategies for constitutive mechanical models using full-field measurements. Int. J. Mech. Sci. 145, 330–345.

Nukala, V., 2016. Buckling of Isotropic and Orthotropic Webs (Ph.D. thesis).

Oberai, A.A., Gokhale, N.H., Goenezen, S., Barbone, P.E., Hall, T.J., Sommer, A.M., Jiang, J., 2009. Linear and nonlinear elasticity imaging of soft tissue in vivo: demonstration of feasibility. Phys. Med. Biol. 54 (5), 1191.

Pan, B., Qian, K., Xie, H., Asundi, A., 2009. Two-dimensional digital image correlation for in-plane displacement and strain measurement: a review. Meas. Sci. Technol. 20 (6), 062001.

Peters, W., Ranson, W., 1982. Digital imaging techniques in experimental stress analysis. Opt. Eng. 21 (3), 213427.

Pierron, F., Grédiac, M., 2012. The Virtual Fields Method: Extracting Constitutive Mechanical Parameters from Full-Field Deformation Measurements. Springer Science & Business Media.

Rensink, M.J., 2012. Through the otoscope: Symptoms poor hearing and wrinkled tissue. Hear. J. 65 (7), 8–10.

Rogers, J.A., Someya, T., Huang, Y., 2010. Materials and mechanics for stretchable electronics. Science 327 (5973), 1603–1607.

Dassault Systèmes SIMULIA Corp, SIMULIA/ABAQUS version 2021. URL https://www.3ds.com/products-services/simulia/products/abaqus/.

Wang, B., Ghanta, P., Vinnikova, S., Bao, S., Liang, J., Lu, H., Wang, S., 2017. Wrinkling of tympanic membrane under unbalanced pressure. J. Appl. Mech. 84 (4), 041002. http://dx.doi.org/10.1115/1.4035858.

Wang, K., Sun, W., 2018. A multiscale multi-permeability poroplasticity model linked by recursive homogenizations and deep learning. Comput. Methods Appl. Mech. Engrg. 334, 337–380.

Zhang, J., Wang, P., Gao, R.X., 2019. Deep learning-based tensile strength prediction in fused deposition modeling. Comput. Ind. 107, 11–21.